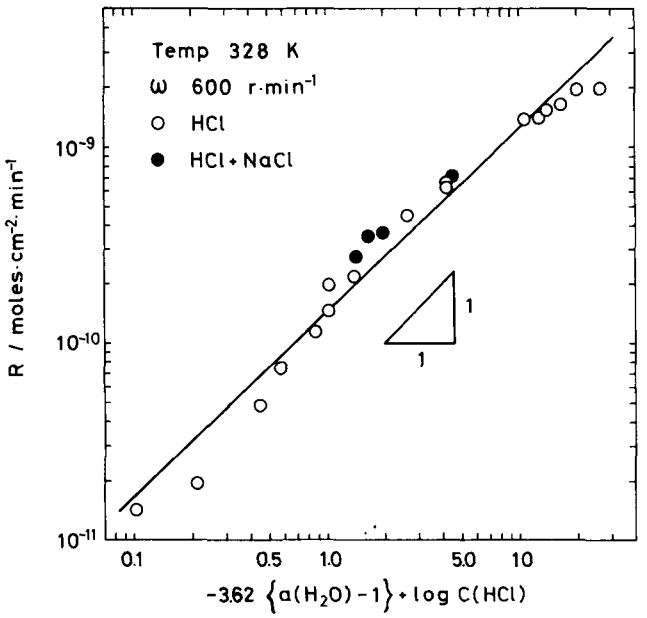

Fig. 4—Relationship between dissolution rate of Fe_2O_3 in acidic chloride solution and $a(H_2O)$ of the solution.

and the parameter $-3.63\{a(H_2O) - 1\} + \log C(HCl)$ on the abscissa (Figures 3 and 4). As these figures clearly show, a linear relationship was detected between log R and $-3.62\{a(H_2O) - 1\} + \log C(HCl)$ for both oxides. The slope of the straight line for CuO was 0.90, while that for Fe_2O_3 was 0.94. These values are sufficiently close to unity.

These findings support the assumption made in this study. Accurate determination of liquid junction potential, and thus rigorous determination of $a(H^+)$ in an acidic chloride solution is impossible. By contrast, the calculation of $a(H_2O)$ value from the concentration data of the component of the solution using the Robinson-Bower equation is simple and accurate, showing only a slight deviation from that experimentally determined. Therefore, when it is desirable to analyze the dissolution reactions of oxide and perhaps sulfide in acidic solutions in terms of $a(H^+)$, Eq. [7] may be useful instead of $a(H^+)$.

REFERENCES

1. H. Majima and Y. Awakura: *Metall. Trans. B*, 1981, vol. 12B, pp. 141-47.
2. H. Majima and Y. Awakura: *Extraction Metallurgy '85*, IMM, London, pp. 607-27.
3. H. Majima, Y. Awakura, T. Sato, and T. Michimoto: *Denki Kagaku*, 1982, vol. 50, pp. 934-40.
4. K. J. Vetter: *Electrochemical Kinetics*, Academic Press, New York, NY, 1967, p. 46.
5. R. A. Robinson and V. E. Bower: *J. Res. Nat. Bur. Stand.*, 1965, vol. 69A, pp. 365-67.
6. H. Majima, Y. Awakura, Y. Takeshima, and K. Sato: *Denki Kagaku*, 1984, vol. 52, pp. 800-71.
7. R. A. Robinson and R. H. Stokes: *Electrolyte Solutions*, 2nd ed., Butterworth Scientific Publications, 1959, appendix 8.10.
8. *Kagaku Binran, Kisohen Part 2*, Nihon Kagaku Kai, ed., Maruzen, Tokyo, 1975.
9. R. G. Bates, B. R. Staples, and R. A. Robinson: *Anal. Chem.*, 1970, vol. 40, pp. 867-71.
10. H. Majima, Y. Awakura, T. Yazaki, and Y. Chikamori: *Metall. Trans. B*, 1980, vol. 11B, pp. 209-14.
11. H. Majima, Y. Awakura, and T. Mishima: *Metall. Trans. B*, 1985, vol. 16B, pp. 23-30.

Possible Roles of Upper Slag Phases on the Fluid Dynamics of Gas Stirred Ladles

D. MAZUMDAR, H. NAKAJIMA, and R. I. L. GUTHRIE

The pouring of liquid steel from a furnace into a ladle, or *vice versa*, generally leads to uncontrolled amounts of slag carryover. Being lighter, this slag separates to form an upper phase of variable thickness and viscosity. While its insulating properties are generally beneficial for maintaining steel temperatures, its chemical characteristics are often detrimental. For instance, steel deoxidation efficiencies can be significantly lowered through chemical reduction of the iron oxide component of any carryover slag. This mass transfer reaction with residual dissolved silicon and/or aluminum deoxidant within the steel can be exacerbated when disturbances of the slag layer during gas bubbling are sufficient to cause slag entrainment. Such stirring procedures have now become standard practice for all concast operations. Tanaka *et al.*[1] have already demonstrated that the high plume velocities associated with gas bubbling can lead to the generation of droplets torn from around the rim of the plume's 'eye' (see Figure 1(b)). However, it is still not known how, and to what degree, the presence of such an upper slag phase affects the various flow variables (*i.e.*, bulk motion, turbulence level, *etc.*) in the bath. These latter parameters must evidently affect the dynamics and efficiencies of metal processing operations in ladles.[2] Indication within the literature suggests[3] that bulk liquid mixing rates may be considerably reduced in the presence of an upper slag. However, neither experimental nor theoretical studies have yet been carried out to rationalize this observation.

Although many theoretical and experimental investigations have now been carried out on the process dynamics of argon stirred ladles (*e.g.*, References 4, 5, 6), numerical as well as physical modeling of such systems has so far tacitly ignored the presence of any overlaying slags. Extrapolation to industrial scale operations[4,5] made on the basis of such idealized situations therefore needs further consideration.

The present work is concerned with developing an understanding of some of the possible ways an upper slag phase may interact with bulk liquid metal during gas injection operations. Water model investigations were therefore carried out as a preliminary step, in which the slag layer associated with actual industrial operations was simulated using commercial grade olive oil (ρ_{oil} = 900 kg/m^3, μ_{oil} = 0.05 kg/m.s.).

Flow phenomena, turbulence characteristics, and the average kinetic energy of motion within the bath were studied as a function of submerged gas flow rate, using a small plexiglass vessel (L = 0.21 m and R = 0.15 m) filled with water. A 15 mm thick layer of olive oil was poured on top

D. MAZUMDAR is Assistant Professor, Department of Metallurgical Engineering, Indian Institute of Technology, Kanpur, India, 208016. H. NAKAJIMA is Assistant Manager, Steelmaking–Continuous Casting, Kashima Works, Sumitomo Metals Industries, Japan. R. I. L. GUTHRIE is Macdonald Professor of Metallurgy, Department of Metallurgical Engineering, McGill University, Montreal, PQ, Canada, H3A 2A7.

Manuscript submitted November 20, 1986.

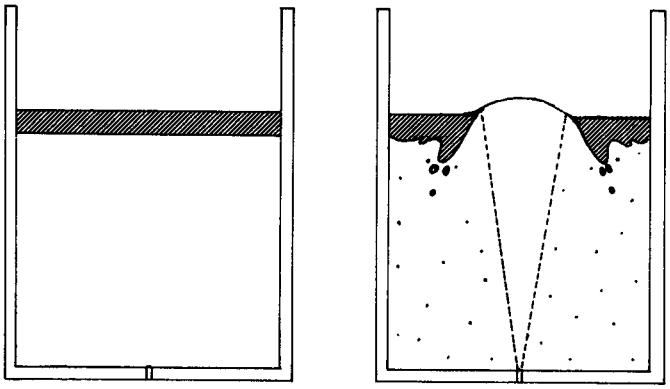

Oil-water system

(*a*) without gas bubbling (*b*) with gas bubbling

Fig. 1—Schematic of equipment used to simulate ladle stirred systems with overlaying slags.

of the water so as to simulate the slag layer of an industrial system. The vessel was provided with a central hole (d = 1.5 mm) at its base, through which air was injected.

Preliminary flow visualization studies were carried out using a suspended network of silken threads. Figure 2, at a gas flowrate of about 1.667×10^{-5} m^3/s, shows that the flows with an upper slag were qualitatively similar to slag-free systems. However, careful examination of the region close to the interface suggests some differences, in that (Figure 2(a)) the subsurface velocities adjacent to free surface are perfectly horizontal, whereas they become deflected downward by about 30 deg with the upper layer present (Figure 2(b)). This indicates that horizontal velocity components near the interface must be considerably damped through interactions of the floating oil phase with the bulk liquid.

Extensive Laser Doppler Velocimetry has been carried out to test this conclusion. Time average and fluctuating components of the flow (*i.e.*, $\bar{u}, \bar{v}, u'$, and v') were measured for a number of gas flow rates at eight different axial positions and at six different radial positions for a total of 48 different locations. Due care was taken to ensure that steady state conditions prevailed during measurements. From these measurements, an average value of the parameter of interest (*i.e.*, the average speed of bath recirculation, U, or average level of turbulence intensity, U', were calculated, using volume weighted averages:

$$\Phi_{av} = \frac{\int_0^L \int_0^R \Phi(I,J) \cdot 2\pi r \, dr \, dz}{\int_0^L \int_0^R 2\pi r \, dr \, dz} \quad [1]$$

$\Phi(I,J)$ represents any scalar ($k, |U|, etc.$) and, Φ_{av} the averaged value of Φ over the entire flow domain. In numerically integrated form Eq. [1] becomes:

$$\Phi_{av} = \frac{\sum_{I=1}^{N} \sum_{J=1}^{M} \Phi(I,J) \cdot \mathrm{Vol}(I,J)}{\sum_{I=1}^{N} \sum_{J=1}^{M} \mathrm{Vol}(I,J)} \quad [2]$$

The results obtained are summarized in Table I. They clearly show that at any gas flow rate, the kinetic energy of mean and fluctuating motion (*i.e.*, the total specific kinetic energy of motion in the system) are considerably reduced by the presence of the top oil phase. To further analyze interactions between the bulk water and oil phases, a 15 mm thick wooden block (D = 0.295 m), floating freely over the liquid water, was used as a replacement so as to simulate a rigid, or pasty, slag. A central hole of dimensions equivalent to that of the exposed eye of the plume was cut, thereby allowing the injected gas to escape. The mean speed of liquid recirculation, average fluc-

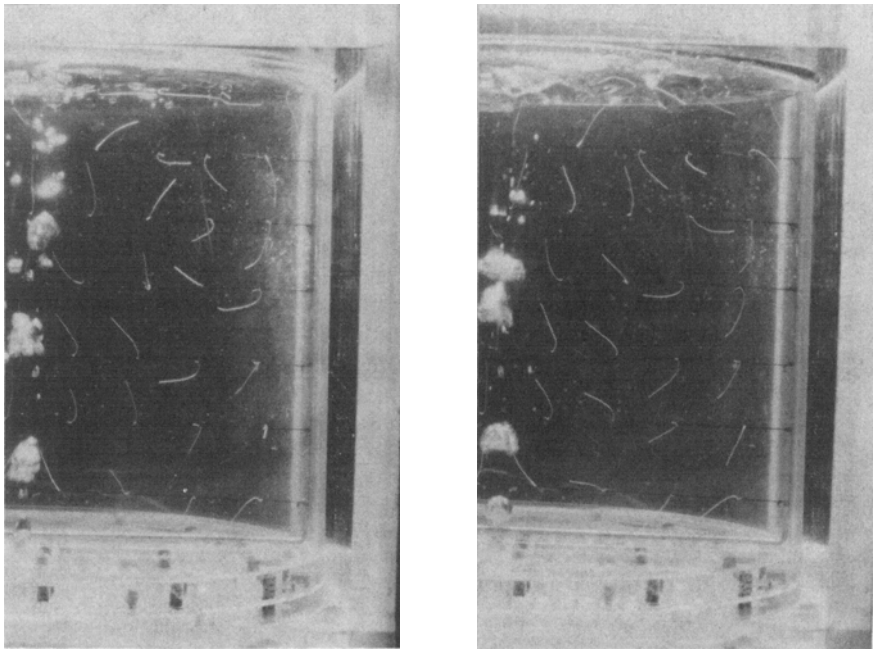

(*a*) (*b*)

Fig. 2—Flow visualization studies using a radial grid of silken threads: (*a*) no overlying oil layer, (*b*) with overlying oil layer.

Table I. Summary of Laser Doppler Anemometry Experiments

Experimental Condition	Gas Flow Rate, m^3/s	Mean Speed of Bath Recirculation mm/s	Mean Fluctuating Velocity in the Bath, mm/s	Total Specific Kinetic Energy of Motion in the Bath J/kg	Specific Energy Input Rate, W/kg
Normal central injection	0.167×10^{-4}	34.0	7.41	6.60×10^{-4}	2.31×10^{-3}
	0.25×10^{-4}	38.25	9.99	8.81×10^{-4}	3.46×10^{-3}
	0.33×10^{-4}	45.45	11.54	12.33×10^{-4}	4.62×10^{-3}
	0.50×10^{-4}	53.42	12.62	16.65×10^{-4}	6.93×10^{-3}
Central injection with an oil layer	0.167×10^{-4}	21.12	6.50	2.84×10^{-4}	2.31×10^{-3}
	0.25×10^{-4}	26.23	7.08	4.19×10^{-4}	3.46×10^{-3}
	0.33×10^{-4}	27.31	8.46	4.80×10^{-4}	4.62×10^{-3}
Central injection with a wooden block at the top	0.167×10^{-4}	30.48	6.10	5.02×10^{-4}	2.31×10^{-3}
	0.250×10^{-4}	37.5	9.19	8.30×10^{-4}	3.46×10^{-3}
	0.330×10^{-4}	41.0	8.40	9.46×10^{-4}	4.62×10^{-3}
	0.50×10^{-4}	49.5	14.85	15.56×10^{-4}	6.93×10^{-3}

Vessel radius = 0.15 m
Liquid depth = 0.21 m

tuating velocity component, *etc.*, for four different gas flowrates obtained under these conditions are also presented in Table I. The three experimental conditions are compared in Figure 3, where the total specific kinetic energy of the bath (*i.e.*, $\frac{1}{2}U^2 + \frac{3}{2}U'^2$) has been plotted against the specific energy input rate ($\simeq$ rate of potential energy input per unit mass *i.e.*, $\rho_L g Q L / \rho_L \pi R^2 L$). It should be noted here that the kinetic energy contribution at the three low gas flow rates (*viz.*, Table I) is less than about 8 pct of the potential energy contribution. However, at the highest gas flow rate ($Q = 5 \times 10^{-5}$ m^3/s), the kinetic energy contribution is higher (~22 pct). In view of the fact that industrial ladle flows are essentially driven by the potential energy of rising bubbles, rather than the kinetic energy of the incoming gas,[4] the contribution of kinetic energy to the overall hydrodynamics has (for simplicity and generality) been omitted from the present analysis. We note that incorporation of a kinetic energy contribution into the estimation of specific energy input rate does not alter the conclusions to be drawn from the present investigation.

Returning to Figure 3, each point essentially represents an average of 48,000 discrete velocity measurements. They clearly demonstrate that the presence of the wooden block over the liquid produced little, or no effect, on fluid flow. This confirms that the mechanism of energy dissipation in the presence of a deformable oil phase is not dominated by the tangential friction generated at a flat two phase interface, as some might anticipate.

With an oil layer, visual observations showed its free surface to be essentially stagnant, but its lower interface with water to be subject to considerable instability and deformation. Further, from the lower rim of the deformed oil mass (see Figure 1), close to the interface, oil droplets formed which subsequently disintegrated into many small droplets (~250 μm diameter). These were carried by convection down into the bulk liquid, despite their natural tendency to refloat to the upper slag phase. Since interfacial friction was shown to have negligible effect on input energy dissipation, other possible mechanisms slowing the mixing process to be considered are:

(1) the surface energy requirements for multiple droplet formation,

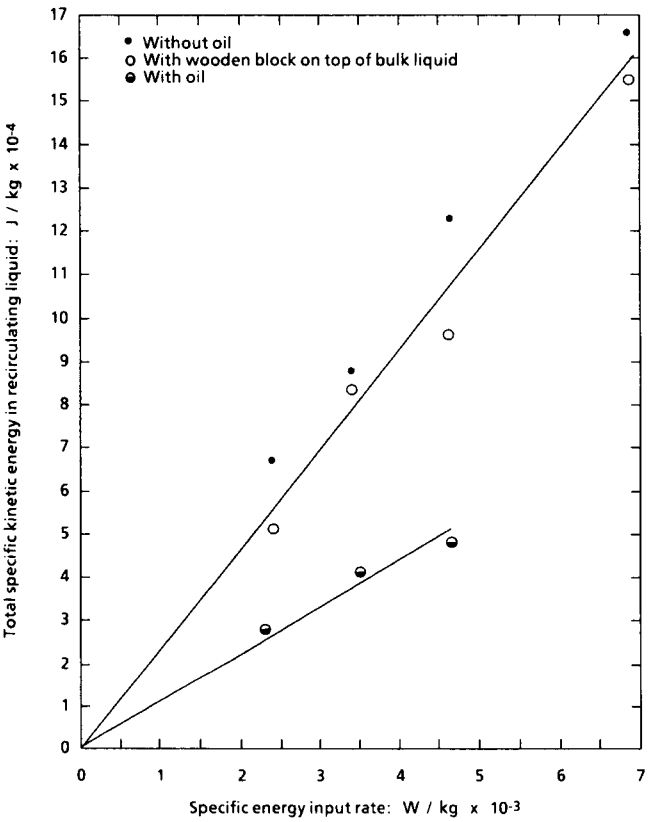

Fig. 3—Plot of total kinetic energy contained in recirculating aqueous phase *vs* energy input referenced to unit mass of liquid, and various 'upper slag phase' conditions, *i.e.*, rigid, fluid, and no-slag conditions.

(2) the potential energy required for keeping these droplets entrained in the lower phase liquid, and
(3) the potential energy required to maintain a deformed oil mass at the oil/water (slag/metal) interface.

Under steady state conditions, the total number of oil particles in the bulk liquid remains dynamically constant, and the number of particles being entrained will equal the number of particles floating up to the oil-water interface. Knowing the number density distribution of droplets, the energy consumed by step (1) is readily estimated (*i.e.*, $E\sigma = n\{4\pi R_p^2\}\sigma$). Thus, the maximum amount of energy

($R_p \sim 250$ μm, $n = 25000$) that could be dissipated by step 1 is about 2×10^{-4} J.

The net potential energy dissipated by the tiny entrained droplets in the bath (step 2) can also be estimated, again provided the total number of such droplets, and their corresponding diameters, are known. The sizes of the entrained oil droplets and their number in the bath at any given flowrate were estimated *via* a novel particle detection device based on the resistive pulse principle.[7] Finally, the energy consumed for step (3) could be estimated through a knowledge of the volume of the deformed oil mass and its mean vertical displacement beneath the oil water interface.

Thus the volume of the deformed oil mass and its downward displacement were deduced through careful visual observation. It was also observed that the thickness of the oil layer on top of the bulk liquid remained practically unchanged during gas bubbling, indicating that the volume of the deformed oil mass under the oil-water interface adjacent to the plume's rising was approximately the same as the volume of oil displaced at the slag's opening (*i.e.*, plume's eye).

For a typical experimental condition ($Q = 0.25 \times 10^{-4}$ m^3/s), the largest entrained droplet size at various locations in the bath was found to be 250 μm, while the total number of such droplets in the bath was approximately 25,000.[8] Taking the mean bath depth as a measure of the average displacement of such particles, the total potential energy contained by these droplets was about 2×10^{-5} J.

On the other hand, at the same gas flowrate, the volume of the deformed oil mass, $V_0 (= \pi R_e^2 l$; $R_e = 0.06$ m and $l = 0.015$ m) was estimated to be 17.0×10^{-5} m^3. The potential energy required to displace the above volume of oil through a mean distance ($= l_o$) of 0.015 m [$= V_0(\rho_L - \rho_{oil})gl_o$] is therefore 25×10^{-4} J. It is interesting to note that only the latter mechanism dissipates energy with a magnitude comparable to that implied by Figure 3 (50×10^{-4} J). Figure 3 also reveals that the kinetic energy of motion within the ladle is proportionately decreased from the 'slag' free case with increasing gas flow. This is presumably the result of a proportionately increasing volume of deformed oil mass and its relatively greater displacement into the bath, as the gas flow rate is increased.

Based on the above information, it is reasonable for one to anticipate that a significant portion of the input energy to a gas stirred ladle can be dissipated by an overlying slag phase, during industrial argon/nitrogen stirring operations. This dissipation of input energy will lead to a decrease in both the mean and turbulence kinetic energies of motion in the bulk steel and may therefore significantly affect the efficiencies of numerous processing operations (*e.g.*, dissolution, dispersion, *etc.*). It is also clear that this dissipation of energy should be related to the thermophysical properties of the slag and its thickness over the liquid melt.

Furthermore, several interesting conclusions can also be deduced on the basis of Figure 3. In the absence of the overlying oil phase, low amplitude ripples can be generated at the free water surface and these will require a continuous input of energy (in the form of potential and surface energy) in order to be sustained. Placing a wooden block over the free water surface virtually eliminates these surface waves, but the specific kinetic energy of motion within the bath was hardly different from the free surface condition. It can therefore be concluded that the presence of the waves at the free surface needs only marginal energy input to be maintained. We should note that this is not true at higher specific gas flowrates such as those encountered in the submerged injection of air into copper converters. Therefore, a significant portion of the input energy is absorbed in splashing and wave formation.[9]

Another interesting conclusion which follows from Figure 3 is the relationship between the quantities plotted along the abscissa and ordinate, respectively. It is evident that a frequency factor relating the quantities plotted along the abscissa (W/kg) and ordinate (J/kg) must exist. Along the abscissa, the rate of potential energy input per unit mass (synonymous to specific energy input rate) has been plotted. In the present context, the specific energy input rate is defined as:

$$\varepsilon_m = \rho_L g Q L / m_L \qquad [3]$$

Replacing Q by fV_B, where f is the bubble frequency and V_B the average bubble volume, the above expression can be rewritten as:

$$\varepsilon_m = (\rho_L g V_B L / m_L) f \qquad [4]$$

One sees that the bracketted quantity now represents a bubble's specific energy input to the system. Following conservation principles, the specific energy input rates of all these bubbles can be expected to be equivalent to the specific kinetic energy of motion within the bath for the 'slag-free' case. Thus, the frequency factor relating the ordinate (J/kg) to the abscissa (W/kg) should represent a 'bubble frequency' parameter. The slope in Figure 3 suggests a 'bubble frequency' in the range of 5 to 10 Hz, similar to that reported for bubbling experiments in liquid iron.[10]

As a final note, the present study suggests that slag phases cannot usually be modeled by assuming the slag-metal interface to be a flat, rigid surface[10] (*i.e.*, a rigid wall boundary treatment) and that a more sophisticated approach is needed for more fluid slags.

In conclusion, slag-metal interactions in industrial operations with reference to argon/nitrogen stirred ladles have been investigated using an oil-water system. These modeling studies show that the overlying oil phase dissipates a part of the input energy, which, in turn, causes the speed of liquid recirculation and the level of turbulence in the bath to be significantly decreased. Three modes of energy dissipation were discussed: 'slag' droplet creation, 'slag' droplet suspension, and 'slag/metal' interface distortion. It was shown experimentally that the third mode, deformation of the overlying oil phase into the lower aqueous phase around the perimeter of the surfacing plume, was primarily responsible for the energy deficit in the recirculating liquid.

LIST OF SYMBOLS

D	Vessel diameter/wooden block diameter, m
d	Orifice diameter, m
f	Bubble frequency, s^{-1}
l	Thickness of 'slag' layer, m
k	Kinetic energy of turbulence per unit mass, m^2/s^2
l_o	Penetration thickness of 'slag' into lower bulk phase around rim of plume
g	Acceleration due to gravity, m/s^2
L	Depth of bulk liquid, m
m_L	Mass of liquid ($= \rho_L \pi R^2 L$), Kg

n Number of particles
N, M Total number of discretized volume elements in the axial and radial direction of the ladle
R Vessel radius, m
R_e Radius of the plume eye, m
$\overline{U}$ Mean axial component of the flow, m/s
U' Fluctuating axial component of the flow, m/s
$\overline{v}$ Mean radial component of the flow, m/s
v' Fluctuating radial component of the flow, m/s
U Mean speed of bath recirculation, m/s
V_B Mean bubble volume, m^3
ε_m Specific energy input rate, W/kg
ρ_L Liquid density, kg/m^3
ρ_{oil} Density of oil, kg/m^3
σ Interfacial tension, N/m

REFERENCES

1. S. Tanaka and R. I. L. Guthrie: *Proceedings, 5th Iron and Steel Congress*, 1986, vol. 6, pp. 249-55.
2. D. Mazumdar and R. I. L. Guthrie: *Metall. Trans. B*, in press.
3. O. Haida, T. Emi, S. Yamada, and F. Sudo: *Proceedings, SCANINJECT II Conference*, Luleå, Sweden, 1980, pp. 20:1-20.
4. Y. Sahai and R. I. L. Guthrie: *Metall. Trans. B*, 1982, vol. 13B, pp. 203-11.
5. D. Mazumdar and R. I. L. Guthrie: *Metall. Trans. B*, 1985, vol. 16B, pp. 83-90.
6. J. H. Grevet, J. Szekely, and N. El-Kaddah: *Int. J. Heat and Mass Transfer*, 1982, vol. 25, no. 4, pp. 487-97.
7. D. Doutre: Ph.D. Thesis, Department of Mining and Metallurgical Engineering, McGill University, Montreal, PQ, 1984.
8. H. Nakajima: Ph.D. Thesis, Department of Mining and Metallurgical Engineering, McGill University, Montreal, PQ, 1986.
9. G. G. Richards, K. J. Legeard, A. A. Bustos, J. K. Brimacombe, and D. Jorgensen: on Innovative Technology and Reactor Design in Extraction Metallurgy, TMS-AIME Fall Meeting, Colorado, Nov. 9-12, 1986.
10. G. Irons and R. I. L. Guthrie: Symp. on Gas Injection into Liquid Metals, University of Newcastle Upon Tyne, England, 1979, pp. C-1-13.
11. N. El-Kaddah and J. Szekely: *Ironmaking and Steelmaking*, 1981, vol. 6, pp. 269-78.

Mass Spectrometric Study of the Activities of the Fe-Ge System at 1550 °C

SHIN-YA NUNOUE and EIICHI KATO

A study of the thermodynamic properties of the Fe-Ge system has been made with the combination of a Knudsen-cell and a mass spectrometer.

A modified commercial mass spectrometer model RM-6K (Hitachi, Japan) was used in the present study. The Knudsen cell which was made of beryllia was 11 mm long and 8 mm inner diameter with a 1.3 mm wall thickness and a 0.5 mm orifice. The alloys were prepared *in situ* by melting together a total of 1.2 to 1.4 g of the component metals in each Knudsen cell. The purities of the metals were 99.9 pct pure iron and 99.999 pct pure germanium. The iron and the germanium were previously deoxidized in a flowing stream of H_2 for 3 hours at 1500 °C and for 3 hours at 1000 °C, respectively. A small amount of beryllium was added to the sample as a deoxidizer. The added amount of beryllium was 0.3 to 1.0 at. pct. In the case of no beryllium added, the ion peak of GeO^+ was observed and the ion current ratio $I_{Fe}{}^+/I_{Ge}{}^+$ was unstable.

The heating of the Knudsen cell was done by the radiation from a helical coil filament of tungsten. The temperature of the Knudsen cell was measured with a Pt-Pt · 13 pct Rh thermocouple attached to the center of the bottom. The temperature of the Knudsen cell was calibrated against the melting point of pure nickel.

The molten alloy was kept for 60 to 120 minutes for the purpose of homogenization of the alloy. The intensities of Fe^+ and Ge^+ were used for checking the homogeneity of the alloy. Measurements were made during sequences of both increasing and decreasing temperature. After a change in temperature, a period of 5 to 20 minutes was usually sufficient to obtain constancy of ion currents for liquid solution.

The experimental results of the ion current ratio for the Fe-Ge system are presented in Figure 1 as a plot of

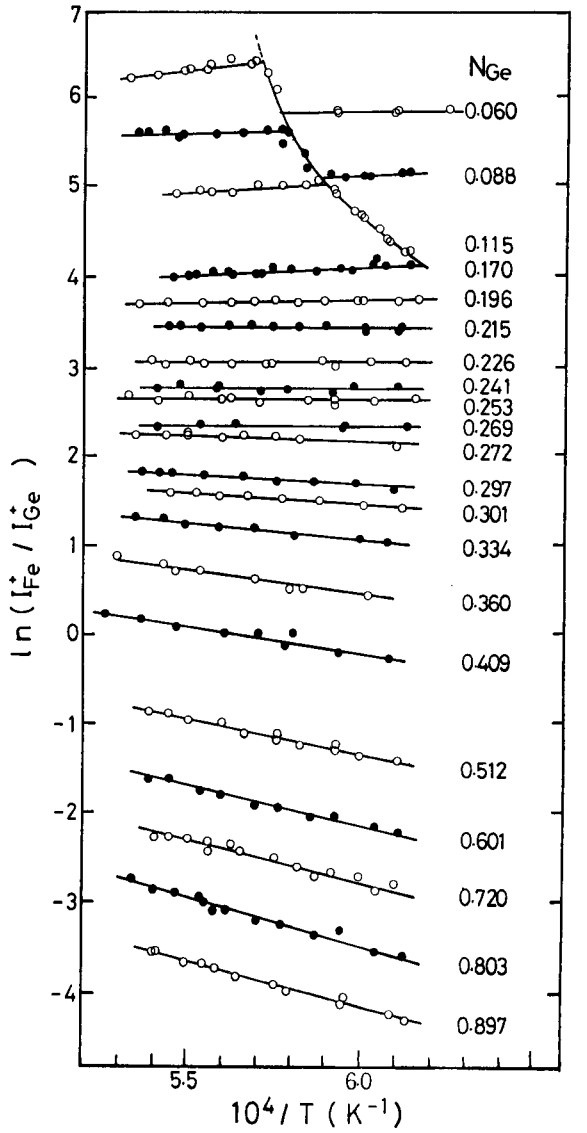

Fig. 1—Temperature dependence of the ion current ratios for the Fe-Ge system.

SHIN-YA NUNOUE, Research Associate, and EIICHI KATO, Professor, are with the Department of Materials Science and Engineering, Waseda University, Tokyo 160, Japan.

Manuscript submitted July 1, 1987.